Granular Mixtures with Tailored Effective Properties

Kianoosh Taghizadeh, Stefan Luding, and Holger Steeb

1 Introduction

In our daily life we are surrounded by granular materials like soil, sand, coffee, nuts, food- or detergent-powders, pharmaceutical products like tablets, and many others. Granular materials constitute over 75% of raw materials feedstock to industry, including pharmaceutical, mining, agriculture, chemical, biotechnological, textile, etc. In spite of their ubiquity and apparent simplicity, their behavior is far from being fully understood. This leads to the loss of about 10% of the world's energy consumption in processing, storage and transport of granular materials, and to various risks related, e.g. to avalanches or landslides due to instability of slopes or foundations.

Granular materials behave differently from usual solids or fluids and show peculiar mechanical properties like dilatancy, history dependence, ratcheting and anisotropy. The behavior of granular materials is highly non-linear and involves irreversibility (plasticity), possibly already at very small strains, due to rearrangements of the elementary particles [1–3]. Furthermore, complex soil behavior also originates from the multi-phase nature of these materials that exhibits both elastic and plastic non-linearities due to solid-fluid coupling.

Mixtures of different type/size particles have become a key research topic in recent years due to their wide range of applications in engineering [4–9], e.g. sand-rubber mixtures in asphalt. The reuse of waste rubber tires creates a win-win situation whereby non-biodegradable tires are given a new lease of life. Understanding gran-

---

K. Taghizadeh (✉) · H. Steeb
Institute of Applied Mechanics (CE), University of Stuttgart, Stuttgart, Germany
e-mail: kianoosh.taghizadeh-bajgirani@mib.uni-stuttgart.de

H. Steeb
e-mail: holger.steeb@mechbau.uni-stuttgart.de

S. Luding
Multiscale Mechanics (MSM), University of Twente, Enschede, The Netherlands
e-mail: s.luding@utwente.nl

P. Eberhard (ed.), *Calm, Smooth and Smart*, Lecture Notes in Applied
and Computational Mechanics 102, https://doi.org/10.1007/978-3-031-36143-2_17

ular mixtures poses still formidable challenges, in particular for complex mixtures with more than one particle species and phase. However, such granular mixtures can exhibit tailored mechanical properties—better than each of the ingredients—due to the interplay of small-big, soft-stiff, and smooth-angular particles.

In analogy to “classical" solids, the behavior of granular materials depends on the amount of deformation the sample is subjected to. Roughly speaking, we can distinguish (i) an elastic regime at very small strain, (ii) a non-linear elasto-plastic regime that holds from small to intermediate strain, and (iii) a fully visco-elaso-plastic regime at large strain and strain rates, where the material flows (solid to fluid transition) at constant stress and volume—if sheared long and fast enough. A special note on the elastic regime should be given: soil behavior is considered to be truly elastic only in the range of extremely small strains ($\varepsilon \leq 10^{-4}$). For slightly higher strain, soil may exhibit a non-linear stress-strain relationship, stiffness being almost fully recoverable when unloading. For larger strain, the material deforms irreversibly and deformations are permanent (plastic). In all cases, the elastic material stiffness is defined only for small strain and can be found from measurements of the (shear) wave velocity in situ and laboratory tests by probing, i.e. incremental stress-strain tests.

Understanding the effective mechanical properties of closely packed, dense granular systems is of interest in many fields, such as soil mechanics, materials science and physics. The main difficulty arises due to discreteness and disorder in granular materials starting at the particle scale, which requires a multi-scale approach. The concept of an initial purely elastic regime at small strains for granular assemblies is an issue still under debate in the soil mechanics community. Approaches that neglect the effect of elastic stored energy are as questionable as approaches that ignore the dynamics.

For many geotechnical structures under working loads, the inherent deformations are small. The regime of deformation where the behaviour can be considered linear elastic is infinitesimal, with nonlinear and irreversible effects present already at small strains. Nevertheless, characterisation of the stiffness of soils is important, as it provides an anchor on which to attach the subsequent stress-strain response [10, 11]. Features visible in experiments, like the propagation of acoustic waves, can hardly be described without considering an elastic regime. Mechanical waves are perturbations moving through space and time in a medium where the small deformations leads to elastic restoring forces. This causes a transfer of momentum or energy through particle contacts without or with little mass transport. The propagation of the mechanical wave through the medium can give valuable information on the state, the structure and the mechanical properties. Through wave propagation with small amplitudes, one can examine a packing without sample disturbance or destruction which makes it possible to probe different situations.

In recent decades, the Discrete Element Method (DEM) has become increasingly popular as a computational tool to model granular systems in both academia and industry [12–14]. To date, due to an increase of computer power, considerable scientific advances have been made in the development of particle simulation methods resulting in an increasing use of DEM. It is a powerful tool to inspect the influence of the microscopic contact properties of the individual constituents on the effective (bulk) behavior of granular assemblies.

The purpose of this contribution is to improve the understanding of basic mechanisms in particle systems and to guide further developments for new macroscopic constitutive models. It is organised as follows: in Sect. 2, the classical relations between wave velocity and elastic moduli in a solid are reviewed; Sect. 3 introduces the wave propagation technique including the interpretation of experimental results; Sect. 4 investigates the effects of inter-particle contact properties on the elastic bulk and shear modulus by applying isotropic and deviatoric perturbations. Further numerical results are compared with experiments. Finally in Sect. 5, we summarise by mentioning the key points of the research and close with an outlook.

2 Waves and Elasticity

A wave is an elastic perturbation that propagates between two material points through a material body (bulk waves) or on the surface (surface waves) without plastic deformation [15]. In the case of bulk waves the acoustic-elastic effect is related to the change in the wave velocity of small amplitude waves due to the stress state of the body.

In the present section, we will review the relations between the elastic characteristics and the velocities of acoustic waves, in the longitudinal and transversal directions [16]. Let us consider a three-dimensional body with density ρ. It is assumed that the material body is homogenous, isotropic and linear-elastic. A volume element subjected to a force F_i in direction i will undertake a displacement ∂u_i in the same direction. The stress change due to the propagation of the wave in the body is given by the local form of the balance of momentum [17]:

$$\frac{\partial \sigma_{ij}}{\partial x_j} = \rho \ddot{u}_i, \tag{1}$$

with the Cauchy stress σ_{ij} and $\ddot{u}_i$ displacement (second time derivative) of the volume element in directions $i, j = 1, 2, 3$. On the other hand, the constitutive relation for the elastic body holds, that relates the stress tensor to the strain ϵ_{ij} via the 4th order elasticity tensor C_{ijkl}

$$\sigma_{ij} = C_{ijkl}\epsilon_{kl}. \tag{2}$$

In the isotropic case, Eq. (2) becomes Hook's law of linear elasticity

$$\sigma_{ij} = \lambda \epsilon_{kk}\delta_{ij} + 2G\epsilon_{ij}, \tag{3}$$

where summation convention is implied $\epsilon_{kk} = \sum_{i=1}^{3} \epsilon_{ii}$, with G and λ the shear modulus and Lamé coefficients respectively, and the linear strain tensor is given by

$$\epsilon_{ij} = \frac{1}{2}\left(\frac{\partial u_i}{\partial x_j} + \frac{\partial u_j}{\partial x_i}\right). \tag{4}$$

The bulk modulus is related to the previous quantities as $K = \lambda + (2/3)G$.

Using Eqs. (3)–(4) in Eq. (1), the equation of motion becomes

$$\rho \frac{\partial^2 u_i}{\partial t^2} = \frac{\partial}{\partial x_j}\left(\lambda \frac{\partial u_i}{\partial x_i}\right) + G\frac{\partial^2 u_i}{\partial x_j^2} + G\frac{\partial}{\partial x_i}\left(\frac{\partial u_i}{\partial x_j}\right). \tag{5}$$

From Helmholtz decomposition, the displacement vector $\boldsymbol{u}$ can be written in terms of a scalar potential ϕ and a vector potential $\boldsymbol{\psi}$: $\boldsymbol{u} = \boldsymbol{\nabla}\phi + \boldsymbol{\nabla} \times \boldsymbol{\psi}$, where the tensorial notation has been used for the sake of brevity. Thus Eq. (5) transforms to

$$\boldsymbol{\nabla}\left[\rho\frac{\partial^2 \phi}{\partial t^2} - \left(\lambda + \frac{4}{3}G\right)\nabla^2\phi\right] + \boldsymbol{\nabla} \times \left[\rho\frac{\partial^2 \boldsymbol{\psi}}{\partial t^2} - G\nabla^2\boldsymbol{\psi}\right] = \mathbf{0}. \tag{6}$$

Equation (6) is known as the wave equation and splits longitudinal and transversal modes of propagation. The first term in Eq. (6) depends only on ϕ, related to propagation of waves in the longitudinal direction, while the second term depends on the vector potential $\boldsymbol{\psi}$, associated with transversal waves. As both terms must be separately zero to satisfy Eq. (6), we obtain the two wave modes for isotropic, homogeneous linear-elastic media. The longitudinal is always faster than the transversal wave mode. Thus, it is also denoted as the P-wave (primary wave). The (slower) transversal wave is known as the secondary wave or S-wave (shear wave).

Finally, if we introduce the longitudinal and shear components of the displacement related to ϕ and $\boldsymbol{\psi}$ as $\boldsymbol{u}_P = \boldsymbol{\nabla}\phi$ and $\boldsymbol{u}_S = \boldsymbol{\nabla} \times \boldsymbol{\psi}$. From Eq. (6) we can derive the velocities of the longitudinal and transversal waves for the isotropic elastic body:

$$V_P = \sqrt{\frac{(\lambda + 4/3G)}{\rho}} \qquad \& \qquad V_S = \sqrt{\frac{G}{\rho}} \tag{7}$$

Note that local rotations do not occur in longitudinal waves at the material point, while volume changes are not present in transversal waves.

The P-wave can move through solids and fluids (as well as gases), like water or the liquid layers of the earth. P-waves are also known as compressional waves, because of the pushing and pulling responses they generate. Subjected to a P-wave, particles move in the same direction as that of the wave moving (shaking the ground in the direction they are propagating). The second type of body wave is the S-wave or secondary wave or shear wave, which is the second wave one can feel in an earthquake (shaking the ground perpendicular to the direction in which they are propagating).

S-waves are slower than P-waves and can only move through solids, not through liquids medium, i.e. shear waves require a medium with shear stiffness to propagate, $G > 0$; thus, they are filtered in fluids. It is this property of S-waves that led seismologists to conclude that the Earth's outer core is a liquid. When observing Eq. (7), some aspects appear: (i) the propagation velocity increases with the stiffness of the material and decreases with its mass density (inertia) these characteristics being constants in a given solid body; (ii) the velocity of transversal waves is smaller than the velocity of longitudinal waves, given the relative values of the moduli; iii) wave velocities of isotropic, homogeneous, linear-elastic media are not a function of frequency, i.e. the medium is non-dispersive.

3 Experimental Study of Small Strain Stiffness

Characterization of mechanical (elasto-plastic) properties has traditionally been made in a triaxial apparatus using precise displacement transducers or in resonant column devices. In recent years, several methods became commercially available to determine the elasto-plastic response of geomaterials both in the laboratory and in the field [18, 19].

The laboratory tests are classified as dynamic or static, as described in Table 1. Dynamic testing is performed at a strain rate high enough to initialize an inertial effect within the specimen, whereas static testing is conducted at a much lower repetition rate at which inertial effects are negligible.

3.1 Wave Propagation Technique

Among experimental characterization techniques, ultrasound wave propagation is widely accepted for their rapid, non-destructive, and low-cost evaluation. Through transmission techniques for determining one-way travelling times, which includes BE (Bender Elements) and UT (Ultrasonic Transducers) technology, has been gaining popularity as an experimental method due to its relative ease of obtaining the modulus of a material. The instrumentation consists of a pair of piezoelectric transducers,

Table 1 List of experiments classified as static or dynamic and their strain levels [20, 21]

	Type of test	Strain (%)
Static	Triaxial (TX)	$>10^{-4}$
Dynamic	Resonant column (RC)	10^{-5}–10^{-2}
	Bender element (BE)	$<10^{-3}$
	Ultrasonic transducer (UT)	$<10^{-4}$

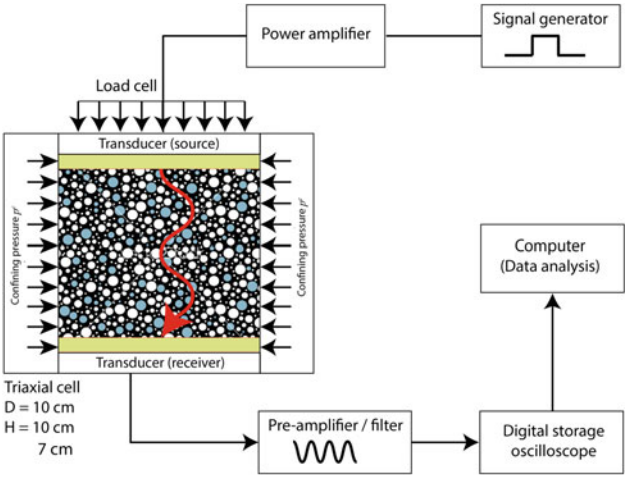

Fig. 1 Schematic drawing of an experimental setup of wave propagation testing [23, 24]

function generator, signal amplifier, voltage divider for the input signals and digital oscilloscope, and signal amplifier/filter. Usually transducers are installed along the axis of the cylindrical sample, i.e. at the top and bottom of a triaxial or oedometric cell, to probe the stiffness of the soil along a given stress path [22]. Figure 1 shows a schematic drawing of the setup and the peripheral electronics. The transmitting transducer transfers the high-voltage electrical signal to a mechanical excitation which is finally propagating through the medium. The receiving piezoelectric transducer receives the propagating mechanical excitation and transforms it back to low-voltage electric signal which will be amplified and acquired with the storage oscilloscope. From the speed-of-sound of the first arrivals and the geometry of the sample, the resulting elastic wave velocities could be obtained. Finally by knowing the elastic wave velocities as measured with the wave-based techniques and total mass density of the media, the stiffness of the materials can be determined.

The signal-to-noise ratio is improved by repetitive averaging of a sufficient number of detected signals using the digital oscilloscope and a computer for further processing. Concerning the travel time (t) and distance (L), necessary to calculate the wave velocity ($V = L/t$), the determination of travel distance (between transducers) is generally considered the less problematic of the two [25, 26].

The longitudinal velocity V_p and the transversal velocity V_s can be measured by using P-wave or S-wave transducers respectively. The longitudinal, P-wave modulus M is related to the P-wave velocity V_p in the medium by

$$M = \rho V_p^2, \tag{8}$$

where ρ is the bulk density of the sample, which is related to porosity ϕ and particle density ρ_p as: $\rho = (1 - \phi)\rho_p$. Note that p stands for rubber or glass, i.e. $p = \{r, g\}$.

3.2 *Procedure and Results*

Uniform glass and rubber particles with similar size (diameter: $d_r = d_g = 4$ mm) are used in this study to prepare cylindrical specimen with different volume fractions of glass and rubber beads.

Glass-rubber samples were prepared with variable rubber content, $\nu = 0$, 0.1, 0.2, ..., 0.9, 1.0, where $\nu = 0$ is composed of glass particles only and $\nu = 1.0$ of rubber particles only [27, 28]. All specimen are tested in our custom-made triaxial cell with sample diameter equal to $D = 10$ cm and two sample heights, $H = 10$ cm and 7 cm. Granular samples are compressed in the axial direction via the top piston in subsequent stress increments. At each step the radial stress is corrected to match the axial stress. Water is used as confining fluid for the samples enclosed by a rubber membrane. At each pressure level (from 50 to 350 kPa), a high voltage burst signal is excited at top to measure the time of flight.

We limit our studies to the compressional P-waves, since the transducers are mounted on the longitudinal direction. The mass density of samples at different rubber content is $\rho = (1 - \nu)\rho_g + \nu\rho_r$, where ρ_g and ρ_r are true mass densities of glass and rubber beads, respectively.

By means of Eq. (8), we can then calculate the P-wave modulus of the granular mixtures tested in the triaxial cell. Figure 2a shows the evolution of the bulk stiffness with the rubber content for all mixtures at different pressure levels. The figure shows that the compressional modulus remains fairly constant by increasing the volume of the rubber content to $\nu = 0.3$. Since the majority of particles are glass, the wave velocity is controlled by glass medium. In the case of high pressure, adding a small amount of soft particles surprisingly enhances the effective P-wave mod-

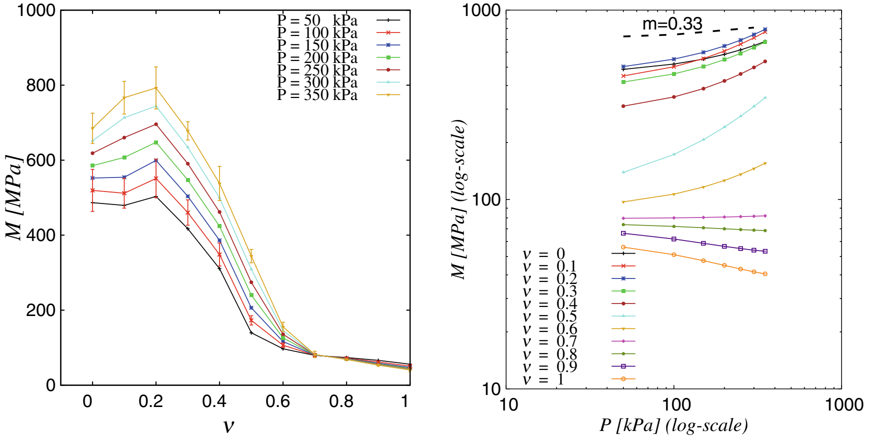

(a)

(b)

Fig. 2 **a** P-wave modulus against rubber fraction. **b** P-wave modulus against confining stress in log-log, see Ref. [33]

ulus measured from longitudinal ultrasound investigations of the medium and the highest modulus is observed at $\nu \approx 0.2$. Thus, granular mixtures can be manipulated to obtain aggregates with even higher stiffness, but lighter and more dissipative, thanks to rubber, when appropriate external conditions are matched (in this case the pressure) [29]. Between $\nu = 0.3$ and 0.6, there is a considerable drop in the wave velocity which is the transition from glass- to rubber-controlled media. Increasing the amount of rubber particles (i.e. the rubber content ν) reduces the effective stiffness. The modulus is again relatively stable between $\nu = 0.6$ to 1 which is linked to the dominance of the rubber media.

In Fig. 2b, M-modulus is plotted against confining pressure p^c (boundary value problem in Fig. 1). The slopes of the M-lines with P are almost constant for $\nu \leq 0.3$ and it follows the expected scaling $M \propto P^{\frac{1}{3}}$ [2, 30, 31]. While the behavior suddenly tends to change by increasing the rubber content (for $\nu = 0.4$ and 0.5). For these samples with intermediate rubber content, the scaling law of the M-modulus with pressure P is $M \propto P^{\frac{1}{2}}$ with a power higher than the typical scaling ($P^{\frac{1}{3}}$). Such a change in the slope is due to the creation of new particle media by incorporating rubber particles [32]. Further on, the modulus becomes almost independent of pressure for higher rubber content. As already observed in Fig. 2a, samples with $\nu = 0.6$ to 1 do not show significant dependence on pressure. The reason for this is related to the softness of rubber particles which deform so high such that they lose the nature of point-to-point contact, i.e. contacts between particles become surface contact.

3.3 Attenuation

When a mechanical wave propagates through a medium, a gradual decay of the wave amplitude can be observed before the wave diminishes, partly for geometric reasons because their energy is distributed on an expanding wave front, and partly because their energy is absorbed or damped by the material they travel through. The energy absorption depends on the material properties. Amplitude is directly related to the acoustic energy or intensity of the travelling ultrasound wave. In certain materials, sound pressure (amplitude) is only reduced by the spreading of the wave. The effect produced is to weaken the sound. ‘Scattering’ is the reflection of the sound waves in directions other than its original direction of propagation. ‘Absorption’ is the conversion of the sound energy to other forms of energy. The combined effect of scattering and absorption is called attenuation of seismic waves and is an important characteristic, e.g. in seismology.

Attenuation is commonly characterized by the quality factor Q. It is most often defined in terms of the maximum energy stored during a cycle, divided by the energy lost during the cycle. Q reflects the energy attenuation of seismic waves in subsurface media as:

$$Q = \frac{Energy\ of\ seisemic\ wave}{Energy\ dissipated\ per\ cycle\ of\ wave} = \frac{2\pi |A(f)|^2}{\Delta |A(f)|^2}, \tag{9}$$

where $|A(f)|^2$ is the energy of the wave, $\Delta|A(f)|^2$ is the change in energy per cycle.

Among various methods [34–40] of measuring attenuation from ultrasound data, the spectral ratio method [41] is most common perhaps because it is easy to use and most stable. Computation of the spectra of the wave and evaluation of the logarithmic ratios for two receivers at depth L_1 and L_2 yields:

$$\ln\left|\frac{A_1(f)}{A_2(f)}\right| = -\frac{\pi(t_2 - t_1)}{Q} f + cte, \tag{10}$$

where $A_1(f)$ and $A_2(f)$ are the amplitude spectra at different lengths, f is the frequency, t_1 and t_2 are the travel time from source to receiver at length L_1 and L_2, and cte is a fitting constant.

To employ the spectral-ratio method for our mixture samples, we perform tests on samples with two different lengths, 7 and 10 cm. As we have found an interesting mechanical response from the stiffness analysis (Fig. 2), we dedicate our attention to samples with low rubber content.

Values of damping (loss factor) Q^{-1} are plotted against the rubber content in Fig. 3a (up to $\nu = 0.3$) for different pressure levels. It is observed that when the amount of rubber increases, the quality factor parameter Q^{-1} decreases with confinig pressure P and increases in a linear fashion, irrespective to the pressure level, i.e. the system is more dissipative by increasing the amount of soft inclusions. Figure 3b demonstrates the systems damping in another fashion where Q^{-1} is plotted versus the confining pressure. As expected, there is a systematical increase of damping by adding soft particle [42, 43]. Combining the observations in Figs. 2 and 3, we summarize that adding roughly about 20% of soft inclusions strongly improves the damping of the system (about 30%), and increases its stiffness (upto 15%) and yet results in a lighter sample (about 15%). Such an effective acoustic behavior of binary mixtures can obviously not be predicted by the application of simple mixture interpolation rules [23].

4 Numerical Modelling—Discrete Element Method

Modelling granular materials can help us to understand their behaviour on the microscopic scale, and to obtain macroscopic continuum relations by a micro- macro transition approach. The Discrete Element Method (DEM) allows to inspect the influence of microscopic contact properties of its individual constituents on the macro bulk behavior of granular assemblies. In this study we use DEM to explore the elastic response of dry frictional granular materials.

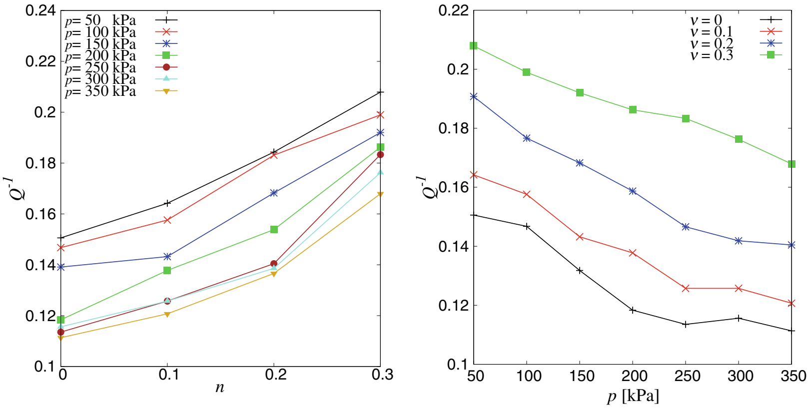

(a) (b)

Fig. 3 **a** Attenuation factor Q^{-1} versus rubber content at different pressure levels and **b** attenuation factor Q^{-1} versus confining pressure for different samples with central frequency of measurement $f \approx 10$ kHz

4.1 Discrete Element Method

If the total force f_i acting on particle i, either due to other particles and boundaries or from external forces, is known, then the problem is reduced to the integration of Newton's equations of motion for the translational and rotational degrees of freedom,

$$m_i \frac{\partial^2}{\partial t^2}\mathbf{r}_i = f_i + m_i g, \quad \& \quad I_i \frac{\mathrm{d}}{\mathrm{d}t}\omega_i = t_i, \tag{11}$$

with m_i the mass of particle i, r_i its position, $f_i = \sum_c f_i^c$ the total force acting on it due to contacts with other particles or with the walls, g the acceleration due to volume forces like gravity, I_i the spherical particle's moment of inertia, ω_i its angular velocity and $t_i = \sum_c \left(l_i^c \times f_i^c + q_i^c\right)$ the total torque, where q_i^c are torques/couples at contacts other than the torques due to the tangential force, e.g., due to rolling and torsion, and l_i^c the vector from the particle's centre of mass to the contact point [14].

The equations of motion are thus a system of $\mathcal{D} + \mathcal{D}(\mathcal{D}-1)/2$ coupled ordinary differential equations to be solved in $\mathcal{D}$ dimensions. The solution of such equations is straightforward, using numerical integration tools such as the ones nicely described in textbooks [44, 45]. The typically short-ranged interactions in granular media allow for further optimizations by using linked-cell spatial structures or alternative methods [44–46] in order to make the search for colliding particles more efficient. In the case of long-range interactions, (e.g. charged particles with Coulomb interaction, or objects in space with self-gravity) this is not possible anymore, so that more advanced methods for optimization have to be applied. Here we restrict ourselves to short-range interactions [47].

Specifically, two spherical particles i and j, with radii a_i and a_j, respectively, interact only if they are in contact, that is, their overlap

$$\delta = (a_i + a_j) - (r_i - r_j) \cdot n \tag{12}$$

is positive, $\delta > 0$, with the unit vector $n = n_{ij} = (r_i - r_j)/|r_i - r_j|$ pointing from j to i. The force on particle i, from particle j, at contact c, can be decomposed into a normal and a tangential part as $f^c := f^c_{ij} = f^n n + f^t t$. In the following, we specify f^c_{ij} for some different models that take into account increasingly complicated grain interactions.

4.2 *Force Laws*

4.2.1 Linear Normal Contact Model

Linear normal forces are the most simple contact laws between two particles [48, 49]. They are based upon a damped harmonic oscillator between two particles and involve a linear repulsive and a linear dissipative force in normal direction:

$$f^n = k\delta + \gamma_0 v_{rel} \tag{13}$$

with a spring stiffness k, a viscous damping γ_0, and the relative velocity v_{rel} in the normal direction $v_{rel} = -(\mathbf{v}_i - \mathbf{v}_j) \cdot \mathbf{n} = \dot{\delta}$. An advantage of the linear contact force law is that the half-period of a oscillation around an equilibrium position resembles the contact duration, $t_c = \pi/\omega$, and can be calculated analytically [50], via:

$$\omega = \sqrt{\frac{k}{m_{ij}} - \left(\frac{\gamma_0}{2m_{ij}}\right)^2} \tag{14}$$

where $m_{ij} = \frac{m_i m_j}{m_i + m_j}$ is the reduced mass and ω is the eigenfrequency of the contact. From Eq. (14) it is possible to obtain the coefficient of restitution which quantifies the ratio of relative velocities after (primed) and before (unprimed) the collision:

$$r_c = \frac{-v'_{rel}}{v_{rel}} = e^{-\frac{\gamma_0 t_c}{2m_{ij}}} \tag{15}$$

For a deeper discussion of the coefficient of restitution and other, more realistic, non-linear contact models, see e.g. [50–52].

The time-step size used in the simulations should be smaller than the contact duration. Here, $\Delta t = \frac{t_c}{50}$ is used for the simulations. Furthermore, notice that in the extreme case of an overdamped spring, t_c can become very large, and therefore the use of neither too weak nor too strong dissipation is recommended.

4.2.2 Hertzian (Non-linear) Contact Force

Instead of linear contact force law, Eq. (13), a non-linear contact force law can be considered, which is based on the elastic contact theory:

$$f^n = E^* \sqrt{d_{eff}} \delta^{\frac{3}{2}}, \tag{16}$$

with $d_{eff} = \frac{4R_i R_j}{R_i + R_j}$ as the effective diameter and the effective Young's modulus for two different material particles $E^* = \frac{2E_i E_j}{E_i + E_j}$.

The linear dissipation used in the linear contact force law can also be applied in the Hertzian contact:

$$f^n = E^* \sqrt{d_{eff}} \delta^{\frac{3}{2}} + \gamma \dot{\delta} \tag{17}$$

Instead of the linear dissipation non-linear options are also available [50]. The Hertzian contact can for example be extended by assuming the material to be non-linierly viscoelastic:

$$f^n = E^* \sqrt{d_{eff}} \delta^{\frac{3}{2}} + \eta \sqrt{\delta} \dot{\delta}, \tag{18}$$

where η is the Hertzian viscosity parameter. This latter force contact law is used in the simulation for the mixtures, as it is known that the linear model represents the experimental dissipation qualitatively wrong as shown in Ref. [50].

4.2.3 Tangential Force Law

The sliding/sticking friction model is based upon Coulomb's law [53]. This law couples the tangential and normal force: For sticking one has static friction $f_t \leq \mu_s f_n$ and for sliding one has dynamic friction, $f_t = \mu_d f_n$. In the static situation a restoring force account for the non-zero tangential force from the surface asperities. To determine if the particle experiences static or dynamic friction a tangential test-force is calculated in the same way as the normal force, which for the linear contact force law gives:

$$f_t = -k_t s - \gamma_t v_{t,rel}, \tag{19}$$

and for the Hertzian normal contact the Mindlin tangential contact force is used:

$$f_t = k_t s \sqrt{d_{eff} \delta} - \gamma_t v_{t,rel}, \tag{20}$$

where k_t is the tangential spring stiffness and s is the relative shear displacement between the two particle centres.

When test-force fulfils $|f_t| \leq f_s^C$ one has static friction. However, when $|f_t| > f_s^C$ is fulfilled, sliding friction becomes active. In Eq. (19) the tangential relative velocity is needed, defined by $v_{t,rel} = v_{ij} - \mathbf{n}(\mathbf{n} \cdot v_{ij})$, where the total relative velocity of the particle surfaces at the contact is given by:

$$v_{ij} = v_i - v_j + a_i' \mathbf{n} \times \omega_i + a_j' \mathbf{n} \times \omega_j \tag{21}$$

with $a_i' = a_i - \frac{\delta}{2}$ is the corrected radius.

4.3 Macroscopic Parameters

4.3.1 Strain

For any deformation, the isotropic part of the infinitesimal strain tensor ϵ_v (in contrast to the true strain ε_v) is defined as:

$$d\epsilon_v = \dot{\epsilon}_v \mathrm{dt} = \frac{\epsilon_{xx} + \epsilon_{yy} + \epsilon_{zz}}{3}, \tag{22}$$

where $\epsilon_{\alpha\alpha} = \dot{\epsilon}_{\alpha\alpha}\mathrm{dt}$ with $\alpha\alpha = xx$, yy and zz as the diagonal elements of the strain tensor ε_{ij} in the Cartesian x, y, z reference system. The integral of $3d\epsilon_v$ denoted by $\varepsilon_\mathrm{v} = 3\int_{V_0}^{V} d\epsilon_\mathrm{v}$, is the true or logarithmic strain, i.e. the volume change of the system, relative to the initial reference volume, V_0 [54].

4.3.2 Stress

From the simulations, one can determine the stress tensor components (compressive stress is positive as convention):

$$\sigma_{ij} = \frac{1}{V}\left(\sum_{p\in V} m^p v_i^p v_j^p - \sum_{c\in V} f_i^c l_j^c\right), \tag{23}$$

with particle p, mass m^p, velocity v^p, neighbouring particles in contact c, force f^c and branch vector l^c, while Greek letters represent components x, y, and z [55, 56]. The first sum is the kinetic stress (energy density) tensor while the second involves the contact-force dyadic product with the branch vector. Averaging, smoothing or coarse graining [57, 58] in the vicinity of the averaging volume, V, weighted according to the vicinity is not applied in this study, since averages are taken over the total volume.

4.3.3 Structural (Fabric) Anisotropy

Besides the stress of a static packing grains, an important microscopic quantity of interest is the fabric/structure tensor. For disordered media, the concept of a fabric tensor naturally occurs when the system consists of an elastic network or a packing of discrete particles. A possible expression for the components of the fabric tensor is provided in [55, 59]:

$$F_{\alpha\beta} = \langle F^p \rangle = \frac{1}{V} \sum_{p \in V} V^p \sum_{c=1}^{N} n_\alpha^c n_\beta^c \,, \tag{24}$$

where V^p is the particle volume of particle p which lies inside the averaging volume V, and n^c is the normal vector pointing from the center of particle p to contact c. $F_{\alpha\beta}$ are thus the components of a symmetric rank two 3×3 tensor.

4.4 DEM Simulation of Small-Strain Stiffness

In this section, we show how to use DEM simulations to study the elastic behavior of granular materials. We use Discrete Element simulations to reproduce static experiments for the characterization of the elastic stiffness of the granular packings.

Table 2 Summary and numerical values of particle parameters used in the DEM simulations

Property	Symbol	Value	Units
Time unit	t_u	1	10^{-6} s
Length unit	x_u	1	10^{-3} m
Mass unit	m_u	1	10^{-9} kg
Particle diameter	$\langle d \rangle$	2	x_u
Polydispersity	d_{max}/d_{min}	3	
Number of particles	N	4096	
Particle density	ρ	2000	m_u/x_u^3
Simulation time step	Δt_{MD}	0.0037	t_u
Normal stiffness	k_n	10^5	m_u/t_u^2
Tangential stiffness	k_t/k_2	0.2	
Restitution coefficient	e	0.804	
Coefficient of friction	μ	[0–10]	
Normal viscosity	$\gamma = \gamma_n$	1000	m_u/t_u
Tangential viscosity	γ_t/γ	0.2	
Background viscosity	γ_b/γ	0.1	

We start our simulations from a set of non-overlapping particles randomly generated in a periodical cubic box at an initial volume fraction $\nu = 0.3$. The initial configuration is compressed isotropically by constant compression strain-rate, $\dot{\varepsilon} = 10^{-4}\ \mathrm{s}^{-1}$, until a given volume fraction $\nu = 0.5$. The system is then allowed to relax at constant volume fraction until it reaches a stable state, which means that the particles dissipate kinetic energy and achieve a zero-pressure. This is followed by an isotropic (slow) compression until the desired maximum volume fraction, $\nu = 0.82$ [60]. The same protocol is used for all samples. For the sake of simplicity, the linear contact model was employed as force law between grains. Parameters used in simulations are summarized in Table 2. In order to investigate the elastic response, we perform so-called strain probing tests in several points along the isotropic preparation (pre-strain) compression path above jamming point (a volume fraction where sample is no longer in fluid-like behavior) [61–63].

Here we consider isotropic prepared samples for which only two independent moduli are needed to characterize the bulk material. The elastic constants K (bulk modulus) and G (shear modulus) are chosen here.

After applying the sufficient relaxation, incremental pure volumetric or pure deviatoric strain are applied to the samples, in order to obtain the bulk and shear moduli, respectively. Isotropic compression of samples is such that samples are homogeneously compressed along all directions; during pure shear, samples are compressed along the x-direction and decompressed along the y-direction, while the z-direction is kept stationary. Shear deformations are applied in the form of a pure shear, i.e., by having a displacement in the y-direction imposed on all particles that cross the x-boundary and a displacement in the x-direction on all particles that cross the y-boundary. One can obtain the samples bulk (K) and shear (G) moduli, by measuring the incremental response to isotropic and shear deformation [60, 61, 64].

Since we apply infinitesimal strain perturbations, we do not expect slippage to occur. However, the friction coefficient is set to infinity ($\mu = \infty$) to prevent any sliding at contacts during probing. For each calculation, we verify that the applied strain is small enough to be in the linear response regime, i.e., the coordination number does not vary during the applied incremental deformation and stress increments are linear proportional to strain increments.

After probing the configurations, the effective elastic moduli of the granular assembly are obtained as the ratio between the measured increment in stress and the applied strain:

$$K^* = \delta P^* / 3\delta\varepsilon_{vol} \qquad \& \qquad G^* = \delta\left(\sigma^*_{xx} - \sigma^*_{yy}\right) / \delta\left(\varepsilon_{xx} - \varepsilon_{yy}\right) \tag{25}$$

where $P^* = Pd/k_n$ and $\sigma^* = \sigma d/k_n$ are the non-dimensional pressure and stress quantities respectively. Hence, K^* and G^* are dimensionless elastic moduli. The advantage of dimensionless moduli is that one can compare samples with different size and type of particles. Results reported later are dimensionless, and for the sake of simplicity, star superscript symbol * is neglected below.

We scan a wide range of inter-particle friction coefficients and volume fractions, and apply small to very large deformations, in order to understand how the interplay of

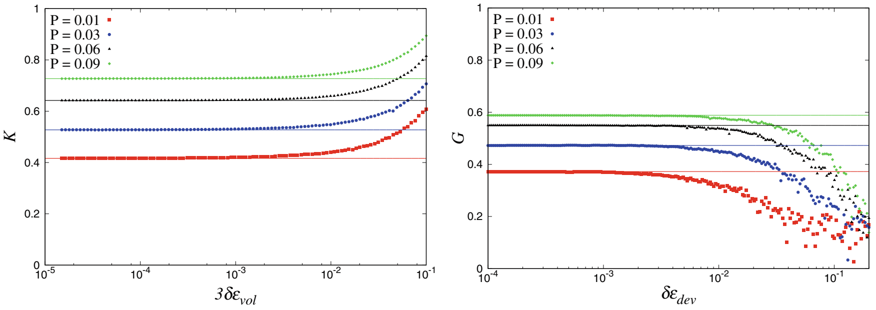

(a) (b)

Fig. 4 Evolution of dimensionless **a** bulk modulus K and **b** shear modulus G with the respective applied isotropic $3\delta\varepsilon_{vol}$ and shear $\delta\varepsilon_{xy}$ strain amplitudes at different pressure $P = 0.01, 0.03, 0.06$ and 0.9, for samples with friction coefficient $\mu = 0.001$. Corresponding dashed lines represent the small strain elastic limit values of K and G

contact and system properties affects the microstructure and thus the elastic moduli. The same procedure is applied for samples created with different values of friction, $\mu = 0 - 10$. As a result, packings at the same density achieve different pressure and microstructure.

As an example, the variation of the bulk and shear moduli with applied strain amplitude is shown in Fig. 4 for $\mu = 0.001$. The elastic moduli stay practically constant for small amplitudes ($3\delta\varepsilon_{vol}$ and $\delta\varepsilon_{xy} < 10^{-4}$ with very slow particles movement rate $\dot{\varepsilon}_{ii} \approx 10^{-5}$) and this can be considered the elastic regime. By increasing the amplitudes of the perturbation, K and G start to increase and decrease non-linearly respectively, i.e. packings are no longer in the elastic regime. The elastic regime becomes larger for higher volume fraction and higher friction (data not shown here) [65].

In Fig. 5, the variations of the bulk K and shear G modulus are plotted with volume fraction for packings with different coefficients of friction μ. As expected, the elastic moduli always increases with increasing density. However, the increase of the moduli is slower for packings with high friction. We can relate this behavior to a lower average number of contacts (i.e. lower volumetric fabric F_v) for samples prepared with higher friction at the same volume fraction. The value of the initial fabric is proportional to the number of contacts, and influences the subsequent evolution of the moduli.

When the elastic moduli are plotted against the isotropic fabric F_v in Fig. 6, the data for the bulk modulus approximately collapse in a unique linear scaling law, implying a general relation between bulk stiffness and isotropic micro-structure: $K = K_0(F_v - F_{v_0})$ with $F_{v_0} \approx 2.2$ and $K_0 \approx 0.1$ for $\mu = 0$ [60] for $\mu > 0$ see [66]. On the other hand, a numerical scaling was not found for the shear modulus G, even if they follow a similar trend with ν. Further investigations are needed. It is worth mentioning that the coefficient of friction has no direct influence on the elastic moduli as sliding is not activated during probing,$\mu_{probing} = \infty$, but rather it effects K and G indirectly through the preparation that leads to a different state variable F_v.

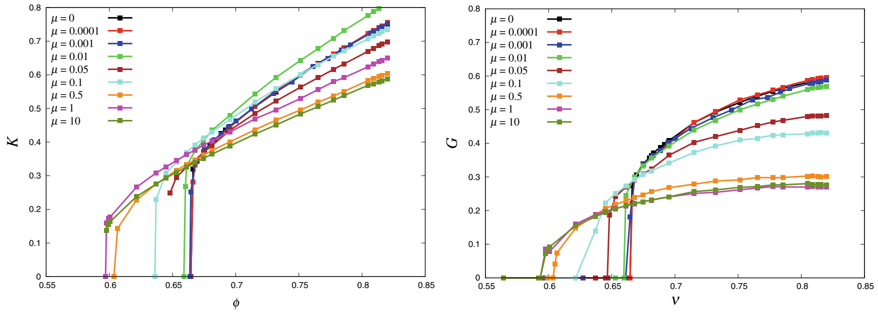

(a) (b)

Fig. 5 Evolution of the normalized **a** bulk modulus K and **b** shear modulus G with volume fraction ν for different coefficients of friction, μ, as shown in the legend

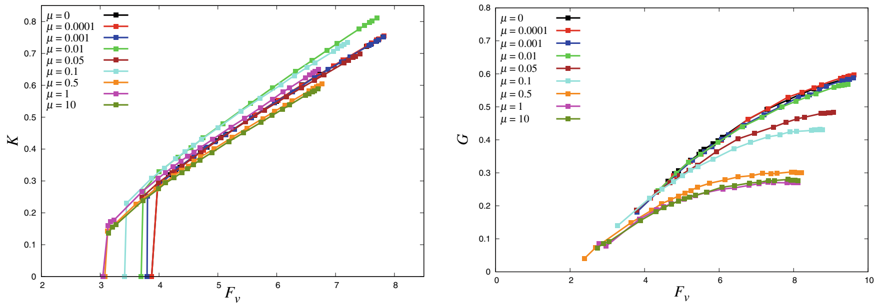

(a) (b)

Fig. 6 Evolution of the normalized **a** bulk modulus K and **b** shear modulus G with volume fraction ν for different coefficients of friction, μ, as shown in the legend

4.5 Comparison Between DEM and Wave Experiments

In this section we show the results of the numerical moduli for different rubber content ν and pressure states. Note that the applied pressure range in simulations is wider than in experiments to gain more insight into the mechanical response of mixtures. Unlike the results shown in the previous section (Sect. 4.4), here the frictional Hertzian contact model was employed for normal contact interactions between two particles; since it captures experimental results better than the linear model. Material properties of glass and rubber are given in Table 3.

In Fig. 7, the P-wave modulus, M, versus pressure is plotted. It is found that the modulus decreases monotonically with the rubber content from $\nu = 0.0$ to $\nu = 1.0$. In this respect, simulations are not able to reproduce the macroscopic behavior observed in Fig. 2, from the experiments with maximum M at $\nu \neq 0$. We associate the mismatch to the adopted contact model not appropriate to properly describe

Fig. 7 P-wave modulus, M, versus applied stress P obtained by DEM simulations

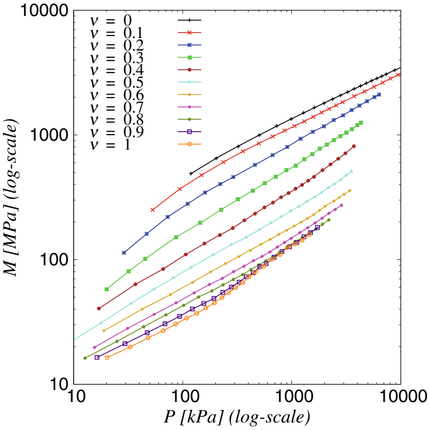

rubber-rubber and rubber-glass interactions. Finding a better contact model is subject to ongoing study. The simulations are not expected to exactly reproduce the experimental observations. Rather, the simulations are valuable because they provide information that is not available in the laboratory tests. However, when experiments and simulations are directly compared in Fig. 8, interesting information can be inferred. For the sake of clarity, only three cases are shown, namely, $\nu = 0.05$, $\nu = 0.5$ and $\nu = 1.0$. Simulations with $\nu = 0.05$ capture the experimental data quantitatively, noticeably without any calibration. On the other hand, when looking at the the packing $\nu = 0.5$, the qualitative trend is well captured by simulations even if actual experimental values are higher than the simulated ones.

Finally, for the case $\nu = 1.0$, where the experimental moduli are pressure independent, simulations are far from experiments in qualitative trend.

By summarizing the previous observations, a three regime scenario shows up. In the glass-dominated regime (G), waves do transmit via a glass beads network, where simulations based on Hertzian interactions are able to reproduce the macroscopic behavior. In the intermediate regime (I) waves still have a preferential path via glass

Table 3 Properties of glass and rubber particles. Further simulation information can be found in Refs. [23, 33, 67]

Used material properties	Glass	Rubber
Diameter (mm)	4	4
Mass density (kg/m^3)	1540	860
Young's modulus (MPa)	65000	1.85
Poisson's ratio	0.24	0.46
Friction coefficient	0.2	0.5

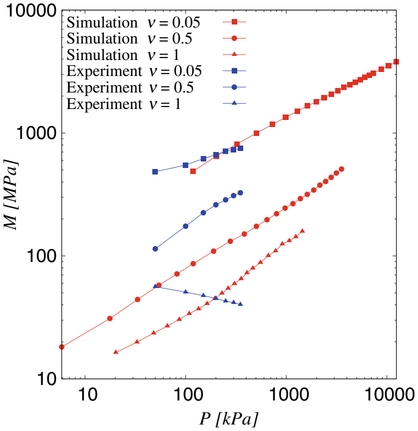

Fig. 8 Experimental and numerical P-wave modulus plotted against pressure; comparison of DEM and experimental glass-rubber mixtures for $\nu = 0.05, 0.5$ and 1.0

bead chains. Here two mechanisms concur to shape the bulk behavior: (i) the density of glass beads in the sample reduces with respect to case G and the actual values of the moduli get lower; (ii) the number of contacts increases with pressure faster than in the G-regime due to easy rearrangement of the rubber particles, that is the slope $M(P)$ gets higher. Finally, in the third regime (R), the behavior of the mixture is dominated by the rubber beads, and the present simple DEM pair contact model cannot offer an accurate representation of the system, because additional high deformation effects need to be considered [67].

5 Summary and Outlook

These days, it has been well understood that grain-scale properties control the bulk-scale behavior of the granular materials. The aim of this contribution was to study and determine the micromechanical mechanisms that govern various phenomena in the world of particles, leading to a better micro-based understanding of the macro-scale response/mechanics of particulate systems.

At first, the elastic response of disordered granular soft-stiff mixtures was investigated experimentally by means of wave-propagation. We found that the behavior is highly non-linear and also non-monotonic with increasing the fraction of soft particles. The uni-axial P-wave modulus is deduced from the linear, uni-axial wave speed and the bulk density of the sample where velocity is the ratio of (variable) sample length and travel time, as measured by the transducers. While it is expected that the stiffness (P-wave modulus) decreases when soft inclusions are replacing the hard particles, interestingly, we observe a nonlinear behavior with a maximum in stiffness at around 20% of soft content, before the stiffness drops and achieves the same rubber-controlled stiffness above 60% soft content.

In contrast to elastic properties, the enhanced dissipative and lightweight properties of the material (like soils, asphalt, etc.) behaves more as expected, when deliberately adding dissipative, soft, light inclusions. This allows for a novel design methodology for calm, smooth, and smart materials that can be better in various aspects than their separate components, e.g., higher stiffness *and* lightweight+damping, at the same time, by adding softer, lighter components.

Numerical simulations using Discrete Element Method (DEM) on the particle scale have revealed the role of the microstructure in characterising the elastic behaviour of granular materials. After preparation by isotropic compression of samples with different inter-particle contact friction, at various volume fraction, the effective elastic moduli are determined from the incremental response by probing isotropic and deviatoric deformations. DEM allows to understand the effects of material parameters, where friction between particles enhances the macroscopic stiffness, while affecting other properties at the same time, such as contact network and coordination number. Thus, selecting/calibrating parameters is an essential task to achieve reliable quantitative agreement with experiments and to allow for predictions for improved materials/designs.

Finally, the P-wave modulus obtained experimentally was compared with the numerical results. While the simulations quantitatively capture the experimental observations for samples at low rubber fraction, the present DEM data show a systematic decrease of the modulus with increasing the rubber fraction unlike the experiments. Future work will focus on improving the contact models towards multi-contact interactions and including the effects of the large deformations of the rubber particles to understand if this improves agreement with experiments; another direction is the extension of our small perturbation approach to elasto-plasticity and then predicting the plastic, irreversible response of a granular assemblies under larger deformation amplitudes.

Acknowledgements Authors acknowledge funding by the German Science Foundation (DFG) through the project STE-969/16-1 within the SPP 1897 “Calm, Smooth and Smart”.

References

1. Bardet, J.P.: Numerical simulations of the incremental responses of idealized granular materials. Int. J. Plast **10**(8), 879–908 (1994)
2. Goddard, J.: Nonlinear elasticity and pressure-dependent wave speeds in granular media. Proc. R. Soc. Lond. A **430**(1878), 105–131 (1990)
3. Sibille, L., Nicot, F., Donzé, F.V., Darve, F.: Analysis of failure occurrence from direct simulations. Eur. J. Environ. Civ. Eng. **13**(2), 187–201 (2009)
4. Heimdahl, T.C., Drescher, A.: Elastic anisotropy of tire shreds. JGGE **125**(5), 383–389 (1999)
5. Hınıslıoğlu, S., Ağar, E.: Use of waste high density polyethylene as bitumen modifier in asphalt concrete mix. Mater. Lett. **58**(3–4), 267–271 (2004)
6. Siddique, R., Naik, T.R.: Properties of concrete containing scrap-tire rubber-an overview. Waste Manage. **24**(6), 563–569 (2004)

7. Xiao, F., Amirkhanian, S., Juang, C.H.: Rutting resistance of rubberized asphalt concrete pavements containing reclaimed asphalt pavement mixtures. J. Mater. Civ. Eng. **19**(6), 475–483 (2007)
8. You, Z., Buttlar, W.: Discrete element modeling to predict the modulus of asphalt concrete mixtures. J. Mater. Civ. Eng. **16**(2), 140–146 (2004)
9. Zornberg, J.G., Cabral, A.R., Viratjandr, C.: Behaviour of tire shred sand mixtures. Can. Geotech. J. **41**(2), 227–241 (2004)
10. Kuwano, R., Jardine, R.: On the applicability of cross-anisotropic elasticity to granular materials at very small strains. Géotechnique **52**(10), 727–749 (2002)
11. La Ragione, L., Jenkins, J.T.: The initial response of an idealized granular material **463**(2079), 735–758 (2007)
12. Taghizadeh, K., Luding, S., Magnanimo, V.: DEM applied to soil mechanics. In: ALERT Doctoral School 2017 Discrete Element Modeling, p. 129 (2017)
13. Cundall, P., Strack, O.: A discrete numerical model for granular assemblies. Géotechnique **29**(1), 47–65 (1979)
14. Luding, S.: Introduction to discrete element methods: basic of contact force models and how to perform the micro-macro transition to continuum theory. Eur. J. Environ. Civ. Eng. **12**(7–8), 785–826 (2008)
15. Aki, K., Richards, P.: Quantitative Seismology. Freeman, New York (1980)
16. Magnanimo, V.: In Wave Propagation and Elasticity in Granular Soils: A Numerical Approach for a Micromechanical Perspective: Views on Microstructures in Granular Materials, pp. 107–135. Springer (2020)
17. David, J., Cheeke, N.: Fundamentals and applications of ultrasonic waves (2017)
18. Clayton, C.: Stiffness at small strain: research and practice. Géotechnique **61**(1), 5–37 (2011)
19. Burland, J.: Ninth Laurits Bjerrum memorial lecture: “small is beautiful”-the stiffness of soils at small strains. Can. Geotech. J. **26**(4), 499–516 (1989)
20. Atkinson, J.: Non-linear soil stiffness in routine design. Géotechnique **50**(5), 487–508 (2000)
21. Lee, C., Shin, H., Lee, J.S.: Behavior of sand-rubber particle mixtures: experimental observations and numerical simulations. Int. J. Numer. Anal. Meth. Geomech. **38**(16), 1651–1663 (2014)
22. Sawangsuriya, A.: In Wave Propagation Methods for Determining Stiffness of Geomaterials: Wave Processes in Classical and New Solids. IntechOpen (2012)
23. Taghizadeh, K., Steeb, H., Luding, S., Magnanimo, V.: Elastic waves in particulate glass-rubber mixtures. Proc. R. Soc. A **477**(2249), 20200834 (2021)
24. Ruf, M., Taghizadeh, K., Steeb, H.: Visualizing particle networks in granular media by in situ X-ray computed tomography (2021). arXiv preprint arXiv:2112.12423
25. Viggiani, G., Atkinson, J.: Interpretation of bender element tests. Geotechnique **45**(1), 149–154 (1995)
26. Lee, J.S., Santamarina, J.C.: Bender elements: performance and signal interpretation. J. Geotech. Geoenviron. Eng. **131**(9), 1063–1070 (2005)
27. Platzer, A., Rouhanifar, S., Richard, P., Cazacliu, B., Ibraim, E.: Sand-rubber mixtures undergoing isotropic loading: derivation and experimental probing of a physical model. Granular Matter **20**(4), 81 (2018)
28. Valdes, J.R., Evans, T.M.: Sand-rubber mixtures: experiments and numerical simulations. Can. Geotech. J. **45**(4), 588–595 (2008)
29. Kim, H.K., Santamarina, J.: Sand-rubber mixtures (large rubber chips). Can. Geotech. J. **45**(10), 1457–1466 (2008)
30. Makse, H.A., Gland, N., Johnson, D.L., Schwartz, L.: Granular packings: nonlinear elasticity, sound propagation, and collective relaxation dynamics. Phys. Rev. E **70**(6), 061302 (2004)
31. Somfai, E., Roux, J.N., Snoeijer, J.H., Van Hecke, M., Van Saarloos, W.: Elastic wave propagation in confined granular systems. Phys. Rev. E **72**(2), 021301 (2005)
32. Bassett, D.S., Owens, E.T., Daniels, K.E., Porter, M.A.: Influence of network topology on sound propagation in granular materials. Phys. Rev. E **86**(4), 041306 (2012)

33. Taghizadeh, K., Steeb, H., Magnanimo, V., Luding, S.: Elastic waves in particulate glass-rubber mixture: experimental and numerical investigations/studies. In: EPJ Web of Conferences, vol. 140, p. 12019. EDP Sciences (2017)
34. Jongmans, D., Campillo, M.: The determination of soil attenuation by geophysical prospecting and the validity of measured Q values for numerical simulations. Soil Dyn. Earthq. Eng. **12**(3), 149–157 (1993)
35. Tonn, R.: Comparison of seven methods for the computation of Q. Phys. Earth Planet. Inter. **55**(3–4), 259–268 (1989)
36. Wang, Z.J., Cao, S.Y., Zhang, H.R., Qu, Y.M., Yuan, D., Yang, J.H., Shao, G.M.: Estimation of quality factors by energy ratio method. Appl. Geophys. **12**(1), 86–92 (2015)
37. Cheng, P., Margrave, G.F.: Estimation of Q: a comparison of different computational methods. CSPG/CSEG/CWLS GeoConvention **12**, 2–5 (2013)
38. Kim, E., Martínez, A.J., Phenisee, S.E., Kevrekidis, P., Porter, M.A., Yang, J.: Direct measurement of superdiffusive energy transport in disordered granular chains. Nat. Commun. **9**(1), 640 (2018)
39. Toksöz, M., Johnston, D.H., Timur, A.: Attenuation of seismic waves in dry and saturated rocks: I. Laboratory measurements. Geophysics **44**(4), 681–690 (1979)
40. Johnston, D.H., Toksöz, M., Timur, A.: Attenuation of seismic waves in dry and saturated rocks: II. Mechanisms. Geophysics **44**(4), 691–711 (1979)
41. Sears, F.M., Bonner, B.P.: Ultrasonic attenuation measurement by spectral ratios utilizing signal processing techniques. IEEE Trans. Geosci. Remote Sens. **2**, 95–99 (1981)
42. Hovem, J.M., Ingram, G.D.: Viscous attenuation of sound in saturated sand. J. Acoust. Soc. Am. **66**(6), 1807–1812 (1979)
43. Cha, M., Cho, G.C., Santamarina, J.C.: Long-wavelength P-wave and S-wave propagation in jointed rock masses. Geophysics **74**(5), E205–E214 (2009)
44. Allen, M.P., Tildesley, D.J.: Computer Simulation of Liquids. Oxford University Press, Oxford (1987)
45. Rapaport, D.C.: The Art of Molecular Dynamics Simulation. Cambridge University Press, Cambridge (1995)
46. Krijgsman, D., Ogarko, V., Luding, S.: Optimal parameters for a hierarchical grid data structure for contact detection in arbitrarily polydisperse particle systems. Comput. Particle Mech. **1**(3), 357–372 (2014)
47. Luding, S., Rivas, N., Weinhart, T.: From soft and hard particle simulations to continuum theory for granular flows. ALERT Geomaterials Doctoral School (2017)
48. Luding, S., Taghizadeh, K., Cheng, C., Kondic, L.: Understanding slow compression and decompression of frictionless soft granular matter by network analysis. Soft Matter **18**(9), 1868–1884 (2022)
49. Taghizadeh, K., Combe, G., Luding, S.: ALERT Doctoral School 2017 Discrete Element Modeling (2017)
50. Luding, S.: In Collisions and Contacts Between Two Particles: Physics of Dry Granular Media, pp. 285–304. Springer (1998)
51. Singh, A., Magnanimo, V., Luding, S.: Mesoscale contact models for sticky particles. Submitted to Powder Technology (2013)
52. Thornton, C., Cummins, S.J., Cleary, P.W.: On elastic-plastic normal contact force models, with and without adhesion. Powder Technol. **315**, 339–346 (2017)
53. Luding, S.: Cohesive, frictional powders: contact models for tension. Granular Matter **10**(4), 235–246 (2008)
54. Göncü, F., Durán, O., Luding, S.: Constitutive relations for the isotropic deformation of frictionless packings of polydisperse spheres. Comptes Rendus Mécanique **338**(10–11), 570–586 (2010)
55. Luding, S.: Anisotropy in cohesive, frictional granular media. J. Phys.: Condens. Matter **17**(24), S2623 (2005)
56. Imole, O.I., Kumar, N., Magnanimo, V., Luding, S.: Hydrostatic and shear behavior of frictionless granular assemblies under different deformation conditions. Kona Powder Part. J. **30**, 84–108 (2013)

57. Weinhart, T., Thornton, A.R., Luding, S., Bokhove, O.: From discrete particles to continuum fields near a boundary. Granular Matter **14**(2), 289–294 (2012)
58. Weinhart, T., Hartkamp, R., Thornton, A.R., Luding, S.: Coarse-grained local and objective continuum description of three-dimensional granular flows down an inclined surface. Phys. Fluids **25**(7), 070605 (2013)
59. Madadi, M., Tsoungui, O., Lätzel, M., Luding, S.: On the fabric tensor of polydisperse granular materials in 2D. Int. J. Solids Struct. **41**(9), 2563–2580 (2004)
60. Kumar, N., Luding, S., Magnanimo, V.: Macroscopic model with anisotropy based on micro-macro information. Acta Mech. **225**(8), 2319–2343 (2014)
61. Magnanimo, V., et al.: Characterizing the shear and bulk moduli of an idealized granular material. EPL (Europhys. Lett.) **81**(3), 34006 (2008)
62. Kumar, N., Luding, S., Magnanimo, V.: Macroscopic model with anisotropy based on micro-macro informatics (2015). arXiv preprint arXiv:1506.02992
63. Calvetti, F., Viggiani, G., Tamagnini, C.: A numerical investigation of the incremental behavior of granular soils. Rivista italiana di geotecnica **37**(3), 11–29 (2003)
64. Taghizadeh, K., Kumar, N., Magnanimo, V., Luding, S.: Understanding the effects of inter-particle contact friction on the elastic moduli of granular materials. In: IOP Conference Series: Earth and Environmental Science, vol. 26, p. 012008. IOP Publishing (2015)
65. Taghizadeh Bajgirani, K.: Elasticity and wave propagation in granular materials. Ph.D. Thesis. University of Twente (2019)
66. Göncü, F., Luding, S.: Effect of particle friction and polydispersity on the macroscopic stress-strain relations of granular materials. Acta Geotech. **8**(6), 629–643 (2013)
67. Giannis, K., Schilde, C., Finke, J., Kwade, A., Celigueta, M., Taghizadeh, K., Luding, S.: Stress based multi-contact model for discrete-element simulations. Granular Matter **23**(2), 1–14 (2021)